PCCP

Accepted Manuscript

ROYAL SOCIETY OF CHEMISTRY

www.rsc.org/pccp

Physical Chemistry Chemical Physics

Non-Radiative Decay Paths in Rhodamines: New Theoretical Insights

Marika Savarese,[a,b] Umberto Raucci,[a] Carlo Adamo,[c,d] Paolo A. Netti,[e] Ilaria Ciofini,[c] and Nadia Rega*[a,b]

Received Xth XXXXXXXXXX 20XX, Accepted Xth XXXXXXXXX 20XX

First published on the web Xth XXXXXXXXXX 200X

DOI: 10.1039/b000000x

We individuate a photoinduced electron transfer (PeT) as a quencing mechanism affecting Rhodamine B photophysics in solvent. The PeT involves an electron transfer from the carboxylate group to the xanthene ring of the Rhodamine B molecular portions. This is finely modulated by the subtle balance of coulombic and non classical interactions between the carboxyphenyl and the xanthene rings, also mediated by the solvent.

We propose the use of an electronic density based index, the so called D_{CT} one, as a new tool to assess and quantify the nature of excited states involved in non-radiative decays near the region of their intersection. In the present case, this analysis allows for getting insights on the interconvertion process from the bright to the dark state responsible for the quenching of Rhodamine B fluorescence.

Our findings encourage the use of density based indices to study processes affecting excited state reactions characterized by a drastical change in the excitation nature in order to rationalize the photophysical behavior of complex molecular systems.

1 Introduction

Recent literature clearly shows how rhodamine dyes, whose general structure is reported in Fig. 1, are founding an increasing number of applications as molecular fluorescence probes in different fields ranging from material science, to chemistry and biology, mainly thanks to their peculiar photophysical properties, such as high photostability, sensitivity and selectivity [1–10]. Nevertheless, in spite of the large amount of experimental and theoretical studies published along the decades, [11–20] a clear and complete picture of the photophysical behavior of rhodamines is far to be fully and unambiguously established. For example, several models have been proposed to rationalize the different quantum yield in molecules belonging to the rhodamine series. Since these dyes have a very low intersystem crossing rate, [12,13] the non-radiative decay should occur through an internal conversion. Nonetheless, there is not a general consensus on which such a reorganization mechanism is. One of the most corroborated theory indicates a structural rearrangement corresponding to a decrease of the C-N bond order upon the $S_0 \rightarrow S_1$ excitation, as the responsible for non-radiative paths opened through the amino groups torsional motions. [16–20] For this reason, rhodamine dyes are usually given as a prototypical examples of the so called Twisted Intramolecular Charge Transfer (TICT) mechanism. [21] Nevertheless, several arguments against the TICT hypothesis exist, [22,23] and other mechanisms have been debated in literature, such as, for instance, the Umbrella Like Mechanism (ULM). [12,14] In particular, recently some theoretical works suggested that a dark state (with strong HOMO-1→LUMO character) can interconvert with the fluorescent state in specific cases such as for the tetramethylrhodamine isothiocyanate in water. [24,25]

Experimentally, and in analogy with what previously observed for the structurally related fluorescein dyes [26], Nagano and coworkers developed Si-Rhodamine-Based NIR fluorescence probes, controlling their fluorescence properties through the tuning of the mechanism of the intramolecular photoinduced electron transfer (PeT). In these Si-Rhodamines a PeT takes place from the phenyl group (acting as the elec-

† Electronic Supplementary Information (ESI) available: [Ground state optimized cartesian cordinates for 5TMR, RhodB, Rhod101; excited state optimized cartesian cordinates for $5TMR_{asym}$, 5TMR, RhodB, $RhodB_{asym}$, Rhod101; energy levels (eV) for 5TMR and $5TMR_{asym}$ computed at the TD-B3LYP-D/6-31G+(d,p)/CPCM level of theory;Complete Reference 45]. See DOI: 10.1039/b000000x/

[a] *Dipartimento di Scienze Chimiche, Università di Napoli 'Federico II', Complesso Universitario di M.S.Angelo, via Cintia, I-80126 Napoli, Italy*

[b] *Italian Institute of Technology, IIT@CRIB Center for Advanced Biomaterials for Healthcare, Largo Barsanti e Matteucci, I-80125 Napoli, Italy*

[c] *Laboratoire d'Electrochimie, Chimie des Interfaces et Modelisation pour l'Energie, CNRS UMR-7575, Ecole Nationale Supérieure de Chimie de Paris,Chimie ParisTech, 11 rue P. et M. Curie, F-75231 Paris Cedex 05, France*

[d] *Institut Universitaire de France, 103 Bd Saint-Michel, F-75005 Paris, France*

[e] *Center for Advanced Biomaterials for Health Care@CRIB, Istituto Italiano di Tecnologia, Largo Barsanti e Matteucci n, 53 80125 Napoli*

* *Tel:+39-081674207; E-mail:nadia.rega@unina.it*

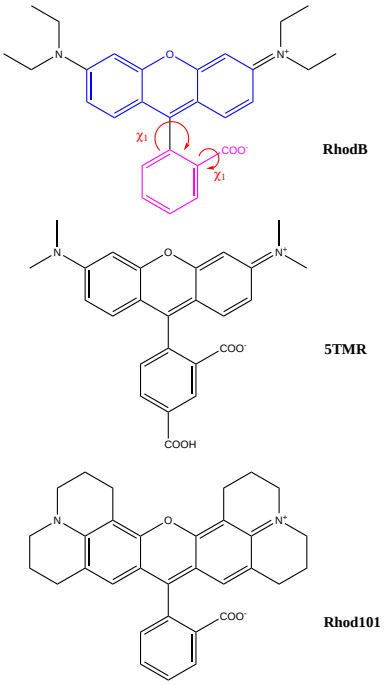

Fig. 1 Schematic structure and labeling of the rhodamines analyzed in this work together with the relevant torsional angles discussed (χ_1 and χ_2)

tron donor moiety) to the xanthene ring (behaving as the electron widthdrawing group).[6,27] More recently, Liu and coworkers discussed the possibility of an intra-molecular PeT occuring in Rhodamine B and its derivatives involving the dialkylated amino groups as electron donors[28], while Yan-qiang and coworkers characterized an ultrafast intermolecular PeT between Rhodamine 101 dye and N,N-diethilanyline from a spectroscopic point of view.[29]

All these experimental observations claim for a higher degree of comprehension of the complex decay pathway(s) taking place in such class of molecules if one aims at obtaining a full control of their photophysical behavior so to achieve a rational design of modern optical sensors.

In this line, recently some of us have combined theoretical approaches, rooted on Time-Dependent Density Functional Theory (TD-DFT), with experimental insights, based on Fluorescence Lifetime Imaging Microscopy (FLIM), to accurately determine and analyze the fluorescence signature (lifetime, quantum yield and band peaks) of several commonly used rhodamine and pyronin dyes.[30]

The present work represents a further step towards the understanding of rhodamine photophysical behavior and it will be entirely devoted to the TD-DFT modeling of the quenching mechanism active in low quantum yield rhodamines such as dialkyl- or tetraalkyl-amino rhodamines. In particular, focusing on three derivatives, namely the Rhodamine B (RhodB), the 5-carboxytetramethyl-rhodamine (5TMR) and the Rhodamine 101 (Rhod101), whose structural formula is schematically illustrated in Fig.1, we will show the importance that an internal conversion to a dark -charge transfer (CT)- excited state may have a non radiative decay path. Remarkably, this non radiative decay can be formally interpreted as an intramolecular PeT from the carboxyphenyl group toward the xanthene one, which is absent in high quantum yield rhodamines.

The modeling of such type of process is far to be trivial from a theoretical point of view, especially at TD-DFT level. The main problem spreads from the correct description of the excited states Potential Energy Surface (PES) in regions close to the crossing points between different electronic states or even in regions where they become very close in energy (near degenerate). As a matter of fact, the Born Oppenheimer approximation breaks down in these regions, the non adiabatic coupling terms becoming infinite at the degenerate points.

In this context, qualitative and quantitative tools enabling the characterization of excited state potential energy surfaces are becoming appealing and promising to help for the in-silico design of new fluorescent probes. Recently, some of us developed a new density based index, the so called D_{CT} index, able to quantify (i.e. give a measure) of the 'degree' of the charge transfer character associated to a given electronic transition[31]. This index, originally devised as a diagnostic tool to identify the erratic behavior of standard DFT approaches in the description of through space CT excitations, has found other applications, such as a measure of the charge separation efficiency of dyes belonging to different push-pull dyes families[31–35] or, more recently, as a simple way to characterize stationary points on excited state PES associated to an Excited State Proton Transfer event.[36].

In the present paper, this index will be used to assess and quantify the nature of the excited states involved in the non-radiative decay near the region of their intersection, and, in particular, to get insights on the interconvertion process to the dark state responsible for the quencing.

The paper is structured as follows: after a brief recall of the methods and computational approaches used (Section 2), the structures and energetic of the minima at the ground and first excited state will be discussed (Section 3). In Section 4, the non radiative decay process will be characterized in term of crossing between two excited state PES corresponding respectively to a locally excited (LE) and a charge transfer (CT) state that will be described both in terms of energy and of density based index. Finally, in Section 5, some general conclusions on the possibility of using TD-DFT and density based indices for the description of critical PES regions and as very promising tools for the rational and controlled design of new fluorescent probes, will be disclosed.

2 Computational Methods and Details

In order to measure the charge transfer character associated to a given electronic transition, a density based index, D_{CT}, easy to compute and simple to interpret, has been recently developed.[31] This index is defined starting from the variation in electronic density associated to a given electronic transitions, $\Delta\rho(r)$:

$$\Delta\rho(r) = \rho_{EX}(r) - \rho_{GS}(r) \quad (1)$$

Two functions can thus be defined ($\rho_+(r)$ and $\rho_-(r)$) collecting the points in the space where an increment or a decrease of the electronic density is produced upon excitation, that is :

$$\rho_+(r) = \begin{cases} \Delta\rho(r) & if \Delta\rho(r) > 0 \\ 0 & if \Delta\rho(r) < 0 \end{cases} \quad (2)$$

$$\rho_-(r) = \begin{cases} \Delta\rho(r) & if \Delta\rho(r) < 0 \\ 0 & if \Delta\rho(r) > 0 \end{cases} \quad (3)$$

It is now possible to individuate the barycenters of the spatial regions defined by $\rho_+(r)$ and $\rho_-(r)$, R_+ and R_- respectively. The D_{CT} represents just the spatial distance between R_+ and R_- and can thus be used to "measure" the CT excitation length:

$$D_{ct} = |R_+ - R_-| \quad (4)$$

Due to the sensitivity of this index on the CT character of a given transition, the D_{CT} will be easily allow to differentiate a CT excited state (possessing a high D_{CT} value) from a Locally Excited State (LE), for which the index value is expected to be low. In order to compute ground and excited state minimal energy structures of the three rhodamine derivatives depicted in Fig. 1, namely RhodB, 5TMR and Rhod101, DFT and TD-DFT were applied using the global hybrid B3LYP functional[37] and including Grimme[38] correction energy terms to account for electronic dispersion interactions (DFT-D).

Solvent (here Acetonitrile) effects were included by the Conductor-like Polarizable Continuum Model (CPCM) in the Linear Response (LR) formalism[39,40] in its equilibrium model[41] when excited state structural optimizations were performed, while the non equilibrium model[42] was applied in all other cases. Structural optimizations were performed at the B3LYP-D/6-31+G(d,p)/CPCM and TD-B3LYP-D/6-31+G(d,p)/CPCM levels of theory for the ground and excited states, respectively.

In order to test that the relative ordering of the excited states is not affected by methodological artifacts related to the use of global hybrids, single point energies for ground and excited states were also computed using the long-range corrected[43] CAM-B3LYP[44] functional.

All calculations were performed with the Gaussian09 suite of programs,[45] but the D_{CT} index was evaluated using a in house developed software, as previously described in literature.[31]

3 Structural and Energetic features at the ground and the excited state

The structural formula of the three rhodamine dyes investigated in this work are reported in Fig. 1 together with their labelling.

In this context it is worth recalling that all rhodamine dyes present a common skeleton constituted by a diamino-xanthene ring with a pendent carboxyphenyl substituent (refer to Fig. 1).

Clearly, the molecules analyzed in this study possess several groups that can be deprotonated so that, as a function of the pH, different charged states are accessible. In this work only the neutral forms of RhodB, 5TMR and Rhod101 have been considered. Two out of the three molecules (namely RhodB and 5TMR) display very low quantum yield as commonly observed for dialkyl- and tetraalkyl- amino and, at variance with other derivatives, the quantum yield of these compounds is also strongly dependent on pH, temperature and viscosity.[14,15,46] On the other hand, the Rhod101 molecule displays a significantly high quantum yield. Quite interestingly, this classification based on low and high quantum yield rhodamines coincides with rhodamines characterized by symmetric and asymmetric S_1 minimum structures, respectively, as discussed by some of us in a previous work concerning a larger set of rhodamine dyes containing 9 molecules.[30] Starting from this observation, we considered the hypothesis that, in symmetrical rhodamines, a quenching internal conversion mechanism could be activated by rotation around the χ_1 and χ_2 torsion angles (refer to Fig. 1 for labeling) leading to a more stable, but dark, excited state. Indeed, both RhodB and 5TMR molecules in the Frank Condon region are characterized by the presence of two closely lying state : a bright Locally Excited (LE) state, centered on the xanthene moiety, and a dark Charge Transfer (CT) state corresponding to a transition from the carboxyphenyl to the xanthene group (see below). Both relative energy of these two states and their intensity are expected to depend on the relative orientation of the two subgroups present in the molecule actually ruled by the χ_1 and χ_2 torsion. Indeed, since χ_1 represents the relative orientation of the phenyl and the xanthene rings, and χ_2 describes the rotation of the carboxy group with respect to the phenyl ring, any change from the $\chi_1 = 90°$ and $\chi_2 = 0°$ arrangement will account for the overall distortion of the two main moieties in rhodamine from the ideal C_s symmetry.

In Tab. 1 values of χ_1 and χ_2 dihedral angles computed for rhodamine optimized in the ground (S_0) and first singlet

	$\|\chi_1\|$		$\|\chi_2\|$	
	S_0	S_1	S_0	S_1
RhodB	94.84	92.26	0.01	0.05
$RhodB_{asym}$	–	62.55	–	19.15
5TMR	94.57	92.37	0.01	4.70
5 TMR_{asym}	–	62.77	–	19.19
Rhod101	117.17	123.87	33.82	39.39

Table 1 χ_1 and χ_2 dihedral angles (in degrees, refer to Fig. 1) computed for rhodamine dyes optimized in the ground (S_0) and first excited singlet (S_1) state at the B3LYP-D/6-31+G(d,p)/CPCM and TD-B3LYP-D/6-31+G(d,p)/CPCM levels of theory, respectively

(S_1) excited states are reported. From these values it is possible to notice that, both at the ground and the first excited state RhodB and 5TMR possess a symmetric structure, with the xanthene and phenyl planes almost perpendicular and the carboxyl group lying in the phenyl plane. On the other hand, the Rhod101 dye is rather unsymmetrical, the carboxyl group being tilted of about 30-40 degrees with respect to the phenyl ring, this latter being far from orthogonality with respect to the xanthene plane.

This type of minimal energy structures, as already noticed for the ground state in a previous work[30], results from the subtle balance between coulombic and non classical interactions involving the two rings which are also modulated by the presence of solvent of different polarity. Indeed, Coulombic attraction and steric repulsion between the polar negatively charged carboxy group and the positively charged xanthene one favor the full symmetrical structure as in the case of RhodB and 5TMR. On the other hand, stabilizing dispersion interactions between the carboxy substituent and the xanthenes may favor an asymmetrical arrangement, as in the case of Rhod101. Furthermore, the overall structure can be modulated by the presence of the polar solvent which may favor conformations displaying a higher exposure of the carboxylic group to the solvent, leading to stabilizing solute-solvent interactions.

Analyzing the vertical transition energies reported in Table 2 it can be noticed that in all cases the first absorption corresponds to a $\pi - \pi^*$ excitation (LE state) centred on the xanthene moiety characterized by a high oscillator strength (intensity). On the other hand, the second electronic transition presents a different character depending on the nature of the amino group carried by the xanthene moiety. In the case of RhodB and 5TMR, this state is of intramolecular CT character, corresponding to a transition from the carboxyphenyl group to the xanthene unit, while in the case of Rhod101 this state is still of LE nature, and it is centred on the xanthene.

Relaxation of the first excited state in the Franck Condon region led to the structures and emission energies reported in Tab. 1 and Tab. 2, respectively. Generally, and in agreement to what previously reported in litterature[30], the level of theory used allows to obtain a good agreement between observed and computed emission energies, with an average error of about 0.15 eV. The nature of the emitting state is further confirmed by the analysis of the associated D_{CT} index. Indeed, in the case of RhodB it results that the distance between the two barycenters of density distribution in the Franck-Condon region is of 1.306 Å and 2.474 Å for the first -relaxed- and second -vertically computed- excited state, respectively (Table 3). These data clearly show the larger electronic density reorganization involved in the case of the second excited state and it allows to confirm its intramolecular charge transfer character, in agreement with the orbital picture discussed for vertical excitation. Therefore, both in the case of RhodB and 5TMR basically in the Franck-Condon region, corresponding to symmetric structure with orthogonal rings, the first relaxed excited state correponds to a bright Locally Excited state (LE) which is found to lye roughly 0.3 eV below a dark CT state. On the other hand, in the case of the asymmetric Rhod101, while the lowest lying state is also of LE character, no closely lying CT states are found.

In order to verify the hypothesis concerning the possibility of a conversion of the bright LE state to a dark CT state by internal rearrangement around $|\chi_1|$ and $|\chi_2|$ in the case of symmetric rhodamines the S_1 structures of RhodB and 5TMR was also optimized starting from an initial distorted guess geometry ($|\chi_1|$=110°, $|\chi_2|$=20°). Starting from this distorted structure, both RhodB and 5TMR relaxed on asymmetrical singlet excited states (here referred to as $RhodB_{asym}$ and 5 TMR_{asym}, respectively) showing clearly asymmetrical structures with $|\chi_1|$ of 118° and 123° for RhodB and 5TMR, respectively, as reported in Tab. 1. From an energetic point of view, these singlet states are characterized by a significantly lower energy with respect to those of the corresponding symmetric structures and by a very low oscillator strength (f=0.004 a.u., Tab. 3), in contrast with the high value of oscillator strenght computed for symmetric excited singlet state minimum discussed above (f=1.22 and f=1.17, Tab. 3).

The analysis of the D_{CT} index computed for these asymmetric singlet states allows to clearly define them as intramolecular CT ones with of D_{CT} 2.599 and 2.546 Å , respectively for RhodB and 5TMR. On the other hand, the -vertically computed- second excited state shows a clear π-π* locally excited state character with D_{CT} of 1.200 and 1.443 Å , respectively. Therefore, both for RhodB and 5TMR not only the two excited states computed in the Franck-Condon region have interconverted upon torsion along the dihedral an-

	S_1			S_2		
	Absorption	Oscillator str.	Character	Absorption	Oscillator str.	Character
RhodB[a]	2.66	f=0.9745	LE	2.96	f=0.1323	CT
5TMR [a]	2.66	f=0.9111	LE	2.98	f=0.1321	CT
Rhod101	2.35	f=1.2563	LE	2.86	f=0.0203	LE

a) Ref. [30]

Table 2 Absorption energies (eV) and oscillator strength (a.u.) of rhodamine dyes calculated at the TD-B3LYP-D/6-31+G(d,p)/CPCM level of theory

	Relaxed S_1			Vertical S_2 at Relaxed S_1 geometry			
	Energy	Oscil. str.	D_{CT}	Energy	Oscil. str.	D_{CT}	Exp.
RhodB	2.41[a]	1.2200	1.201	2.76	0.1504	2.474	2.18[b]
$RhodB_{asym}$	1.45	0.0300	2.599	2.34	1.0862	1.200	
5TMR	2.40[a]	1.1706	1.375	2.77	0.1554	2.477	2.18[b]
5 TMR_{asym}	1.51	0.0432	2.546	2.29	0.9722	1.443	
Rhod101	2.25	1.1904	1.672	2.71	0.0006	2.631	2.06[c]

a)[30] b) Ref.[47]; c) Ref.[28]

Table 3 Relaxed S_1 and vertical S_2 excited state energies (in eV) of rhodamine dyes calculated at the TD-B3LYP-D/6-31+G(d,p)/CPCM level of theory. Available experimental values are reported for comparison

gles but also, the LE/CT state shows a sizable (about 0.1 Å) decrement/increment of in the electronic density reorganization upon transition. Furthermore, due to the strong stabilization of the dark CT state, the energy difference between the first and the second excited state increases up to roughly 0.9 eV for both RhodB and 5TMR in their asymmetric geometry. In the case of Rhod101 on the other hand starting from a symmetric or asymmetric guess structure for the optimization of the first excited state has no impact on the final results, always corresponding to the same LE distorted structure as reported in Tab. 1 and Tab. 3. This is due to the absence of a closely lying CT state which maybe sufficiently stabilized by a structural distorsion.

4 Non-radiative decay process

In order to further investigate the possibility of conversion of the bright LE into the dark CT state upon rotation around the χ_1 and χ_2, in the case of rhodamines presenting a symmetric ground state structure, a linear synchronous path (LSP) consisting of 20 points linking the symmetrical and asymmetrical excited state minima for RhodB was constructed. For each of these structures the second excited state was vertically computed. Basically, this linear synchronous coordinate (c_{LSP}) represents the structural evolution from the symmetrical Franck Condon region (c_{LSP}=0), where the emitting state is a bright LE one to the asymmetrical minimum (c_{LSP}=1) corresponding to a dark CT state. In order to define the nature of the excited states the D_{CT} index was computed for both first and second excited state for all points along the path. The computed energy profiles associated to the first and second excited states are reported in Fig. 2 while the associated D_{CT} are reported in Fig. 3.

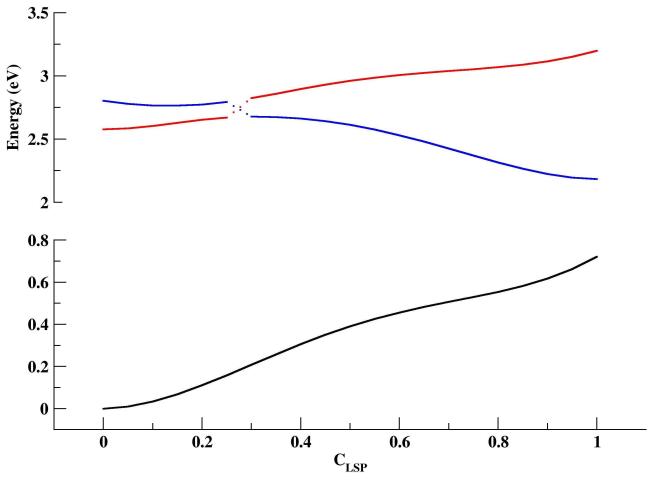

Fig. 2 Evolution the energy associated to the LE and CT excited states (in eV) of RhodB along the LSP connecting the symmetrical (c_{LSP}=0) to the asymmetrical c_{LSP}=1 excited state minima

From the analysis of these figures it is clear that the two excited states cross in the region around c_{LSP}=0.25, the detailed study of the crossing being clearly impossible at the level of theory here applied. Indeed, from the combined analysis of the D_{CT} it is possible to point out that in the crossing region also the character of the transitions is inverted. The first excited

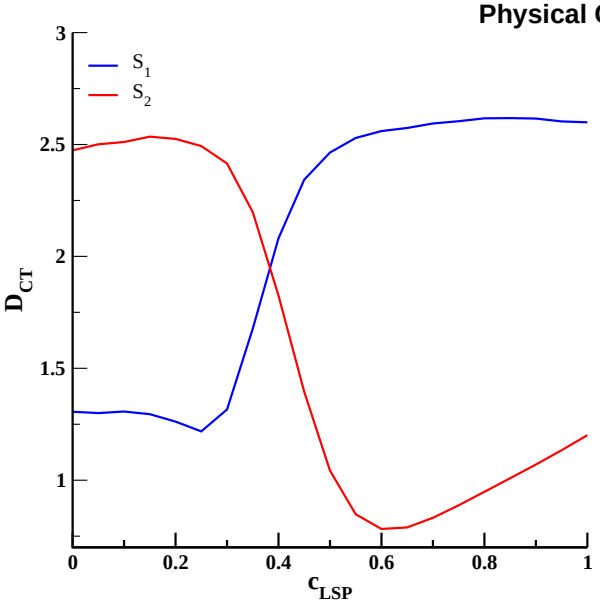

Fig. 3 Evolution of the D_{ct} (in Å) associated to the first S_1 and second S_2 excited states computed along the LSP connecting the symmetrical (c_{LSP}=0) to the asymmetrical (c_{LSP}=1) excited state minima of RhodB

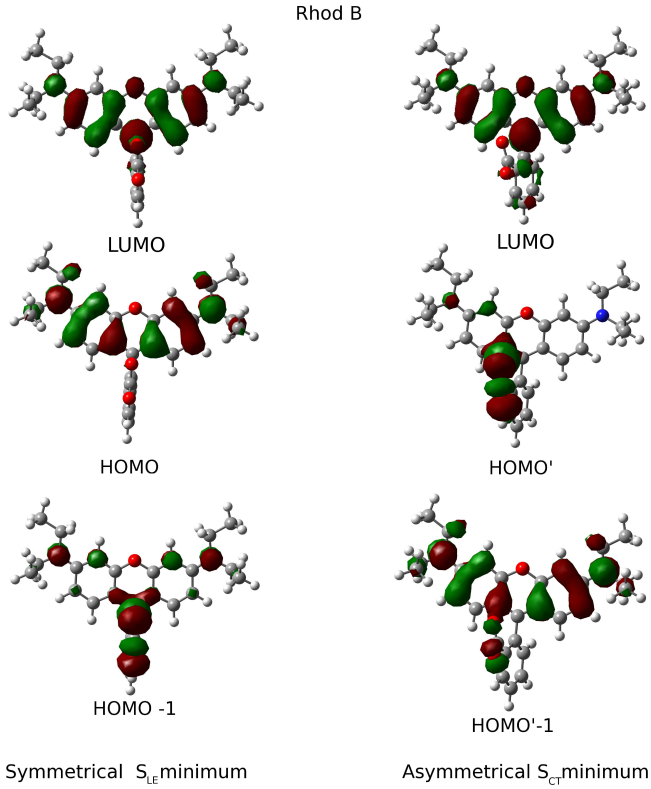

Fig. 4 LUMO, HOMO and HOMO-1 computed for symmetrical and asymmetrical RhodB structures corresponding to the optimized first singlet excited state

state showing a more local character, translating into a lower D_{CT} value, in the case of symmetric structures becomes of a more marked CT character moving towards the asymmetric minimum (c_{LSP}=1). The inversion of the two states thus allows for the conversion of the emissive bright LE state present in the Franck Condon region to the dark CT and more stable distorted minimum thus justifying a low yield for this compound.

Nonetheless the question still unanswered is related to the electronic reason that causes the inversion of the excited states. Analysis of the molecular orbitals mainly involved in the one-electron excitations describing at TD-DFT level the excited states for RhodB, allows clarifying for this point. Actually, at any point of the LSP, the first (or second) excited state corresponds essentially to a one electron excitation from the HOMO (or HOMO-1) to LUMO. While the LUMO (reported in Fig. 4) is completely insensitive to the structural rearrangement occurring along the LSP and keeps always the same nature (localized on the xanthene unit) and energy, this is not the case for the HOMO and HOMO-1 as shown in Fig. 4. For the symmetric structure, the HOMO is essential a π xanthenic orbital with associated orbital energy (ε) of -0.211 a.u., while the HOMO-1 is mainly localized on the carboxylate group on the phenyl substituent lying roughly 0.018 a.u. below the HOMO. As a consequence the HOMO→LUMO excitation leads to the LE first excited state responsible for the radiative decay providing fluorescence. The HOMO-1→LUMO excitation, on the other hand, leads to a dark CT excited state.

Considering the asymmetrical minimum (c_{LSP}=1), we notice that the HOMO and HOMO-1 actually corresponds to carboxylate and xanthene centered orbitals, respectively with corresponding ε values of -0.195 a.u. and -0.218 a.u. That means that the HOMO and HOMO-1 have inverted with respect to the symmetrical minima. This inversion is related mainly to the strong destabilization of the doubly occupied carboxylate centered orbital while the xanthene centered one is actually almost unaffected. The destabilization of the carboxylate orbital is related to the increasing repulsion with the xanthene π systems which is also responsible for the increase in the total energy of the ground state of the molecule. Therefore molecular vibrations, in particular those involving the relative orientation of the xanthene and phenyl rings, promote the PeT quenching mechanism, affecting the energy gap between the LE and CT electronic states and creating the non adiabatic coupling between them. This connection has been recently proven by non-adiabatic molecular dynamics to describe a PeT from PbS Quantum Dots to RhodB molecules.[48]

Noteworthy, the frontier orbitals inversion when going from a symmetrical to an asymmetrical arrangement can be schema-

tized as an hole transfer from the xanthene to the carboxylate moiety at the excited state as shown in Fig. 5.

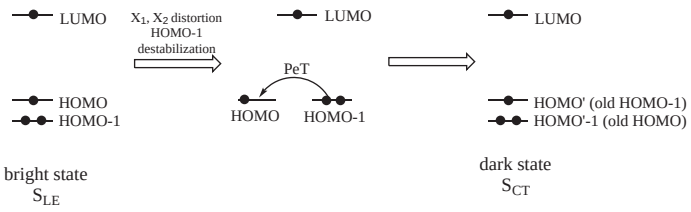

Fig. 5 Scheme of the photo induced electron transfer mechanism active in RhodB

In this simplified orbital picture, the starting first excited state is the bright state LE state populated in the Franck Condon region, schematically represented by singly occupied HOMO and LUMO and a doubly occupied HOMO-1. Upon relaxation, corresponding to the distortion of xanthene and phenyl rings, the HOMO-1 undergoes a destabilization and eventually switches with the HOMO. This orbital interchange actually allows an electron transfer from new HOMO (previously HOMO-1) to HOMO-1 (previously HOMO), leading to the final dark state.

The quenching mechanism described above is triggered by the destabilization of carboxylate group orbital so that this mechanism should be active in principle for all rhodamines. Indeed, for rhodamines that show no contribution stemming from the carboxylate group to the lowest lying excited state, this quenching mechanism is completely negligible. This is actually the case of all asymmetric rhodamines since in such case the carboxy group always contributes to more internal orbitals. As an example, in Fig. 6 the HOMO-1 computed for the symmetric structure of RhodB, 5TMR can be compared to that computed for the Rhod101.

For the latter system (Rhod101), at variance with dialkyl- and tetraalkyl- amino rhodamines, the HOMO-1 in mainly localized on the xanthene ring. It is reasonably to assume that in this case the above discussed quenching mechanism is precluded and this is also the reason why a single minima on the first excited state potential energy surface of LE character is found, always corresponding to a distorted structure.

In order to check that the mechanisms are results discussed above are not affected by methodological artifacts related to the used of a global hybrid functional (B3LYP) for the description of the relative energy of CT and LE state, CAM-B3LYP calculations were also performed on the symmetric and asymmetric excited state[43]

The results obtained at the TD-CAM-B3LYP/6-31G+(d,p)/CPCM level in acetonitrile qualitatively producing the same picture and discussed above, confirm our analysis.

In this context it is worth recalling that, the accuracy of global hybrids such as B3LYP in the description of CT states

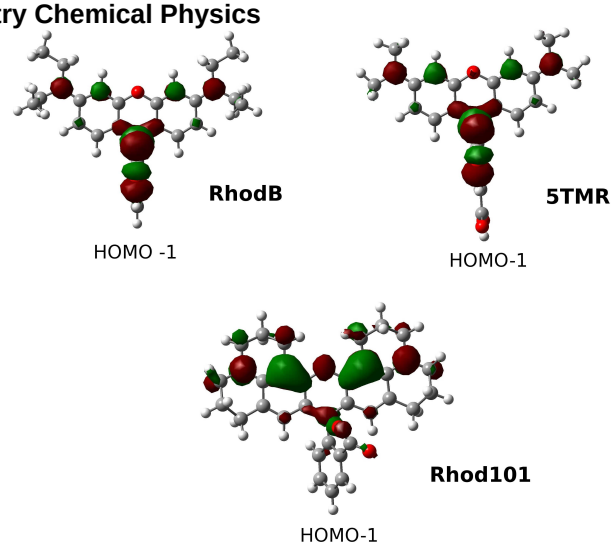

Fig. 6 HOMO-1 orbitals computed for RhodB, 5TMR and Rhod101 their Franck Condon first excited state minimum energy structure (symmetric structure for RhodB and 5TMR; asymmetric structure for Rhod101

when combined with LR-PCM has been previously reported and analyzed.[49,50] Indeed, the good results obtained are probably ascribable to an error compensation since global hybrid functionals over-stabilize CT excitations while the linear response treatment of the solvent leads to an under-stabilization of states characterized by a large change of the electric moment, such is the case of CT states.[40].

5 Conclusions

A possible non radiative decay pathway able to explain the different quantum yield observed for different type of rhodamine dyes has been investigated and supported by theoretical analysis of the ground and excited state potential energy surfaces performed at DFT and TD-DFT level. This mechanism, active for rhodamines where two different excited state of bright (LE) and dark (CT) character are sufficiently close in energy in the Franck-Condon region, is triggered by a structural deformation involving the mutual rotation of the xanthene and carboxyphenyl moieties and it can be schematically interpreted as an intramolecular Photo-induced electron tranfer. Beside the possibility of using the theoretical tools here applied to the modeling of other emission processes, more interestingly we hope that the elucidation of this non-radiative decay path may help the design and synthesis of new systems and, in particular, of rhodamines with enhanced emission properties obtained by the suppression of this de-activation pathway by chemical modification (such as inclusion of bulky, but electronically inhert substituent or by ridigification of the molecular skeleton).

Acknowledgments

N.R., M.S. and U.R. acknowledge the financial support from Gaussian Inc. and MIUR, PRIN prot.2010*FM*738*P*_002

References

1 N. Yapici, S. Jockusch, A. Moscatelli, S. Mandalapu, Y. Itagaki, D. Bates, S. Wiseman, K. Gibson, N. Turro and L. Bi, *Org. Lett.*, 2012, **14**, 50–53.
2 M. Kumar, N. Kumar, V. Bhalla, P. Sharma and T. Kaur, *Org. Lett.*, 2012, **14**, 406–409.
3 Z. Yang, M. She, B. Yin, J. Cui, Y. Zhang, W. Sun, J. Li and Z. Shi, *J. Org. Chem.*, 2012, **77**, 1143–1147.
4 Y. Koide, Y. Urano, K. Hanaoka, W. Piao, M. Kusakabe, N. Saito, T. Terai, T. Okabe and T. Nagano, *J. Am. Chem. Soc.*, 2012, **134**, 5029–5031.
5 M. Beija, C. Afonso and J. Martinho, *Chem. Soc. Rev.*, 2009, **38**, 2410.
6 Y. Koide, Y. Urano, K. Hanaoka, T. Terai and T. Nagano, *ACS Chem. Biol.*, 2011, **6**, 600–608.
7 D. R. Larson, H. Ow, H. D. Vishwasrao, A. A. Heikal, U. Wiesner and W. W. Webb, *Chem. Mat.*, 2008, **20**, 2677–2684.
8 K. Chingin, R. M. Balabin, V. Frankevich, H. Chen, K. Barylyuk, R. Nieckarz, A. Fedorov and R. Zenobi, *Phys. Chem. Chem. Phys.*, 2010, **12**, 14121.
9 K. Chingin, R. M. Balabin, K. Barylyuk, H. Chen, V. Frankevich and R. Zenobi, *Phys. Chem. Chem. Phys.*, 2010, **12**, 11710.
10 E. Kato and T. Murakami, *Polymer Gels and Networks*, 1998, **6**, 179–190.
11 F. L. Arbeloa and K. K. Rohatgi-Mukherjee, *Chem. Phys. Lett.*, 1986, **129**, 607–614.
12 F. L. Arbeloa and I. U. Aguirresacona, *Chem. Phys.*, 1989, **130**, 371–378.
13 A. Penzkofer and M. Falkenstein, *Opt. Quant. Electron*, 1978, **10**, 399–423.
14 M. Snare, F. Treloar, K. Ghiggino and P. Thistlethwaite, *J. Photochem.*, 1982, **18**, 335–346.
15 T. Karstens and K. Kobs, *J. Phys. Chem.*, 1980, **84**, 1871–1872.
16 K. H. Drexhage, *Top. Appl. Phys.*, 1973, **1**, 144.
17 K. Drexhage, *J. Res. Natl. Bur. Stand*, 1976, **80**, 421–428.
18 K. Drexhage, *Dye lasers*, 1973, 155–200.
19 M. W. Vogel, W. Rettig, R. Sens and K. H. Drexhage, *Chem. Phys. Lett.*, 1988, **147**, 452–460.
20 Z. Grabowski, K. Rotkiewicz, A. Siemiarczuk, D. J. Cowley and W. Baumann, *Nouv. J. Chim.*, 1979, **3**, 443–454.
21 Z. R. Grabowski, K. Rotkiewicz and W. Rettig, *Chem. Rev.*, 2003, **103**, 3899–4032.
22 K. A. Zachariasse, T. von der Haar, A. Hebecker, U. Leinhos and W. KUhnle, *Pure Appl. Chem.*, 1993, **65**, 1745–1750.
23 T. von der Haar, A. Hebecker, Y. Il'ichev, Y. B. Jiang, W. Ktihnle and K. A. Zachariasse, *Recl. Trav. Chim. Pays-Bas*, 1995, **114**, 430–442.
24 A. Pedone, G. Prampolini, S. Monti and V. Barone, *Chemistry of Materials*, 2011, **23**, 5016–5023.
25 V. Barone, J. Bloino, S. Monti, A. Pedone and G. Prampolini, *Phys. Chem. Chem. Phys.*, 2011, **13**, 2160–2166.
26 T. Miura, Y. Urano, K. Tanaka, T. Nagano, K. Ohkubo and S. Fukuzumi, *J. Am. Chem. Soc.*, 2003, **125**, 8666–8671.
27 Y. Koide, Y. Urano, K. Hanaoka, T. Terai and T. Nagano, *J. Am. Chem. Soc.*, 2011, **133**, 5680–5682.
28 X.-F. Zhang, Y. Zhang and L. Liu, *J. Lumin.*, 2014, **145**, 448–453.
29 L.-l. Jiang, W.-l. Liu, Y.-f. Song, X. He, Y. Wang, C. Wang, H.-l. Wu, F. Yang and Y.-q. Yang, *Chemical Physics*, 2014, **429**, 12–19.
30 M. Savarese, A. Aliberti, I. De Santo, E. Battista, F. Causa, P. A. Netti and N. Rega, *J. Phys. Chem. A*, 2012, **116**, 7491–7497.
31 T. Le Bahers, C. Adamo and I. Ciofini, *J. Chem. Theory Comput.*, 2011, **7**, 2498–2506.
32 I. Ciofini, T. Le Bahers, C. Adamo, F. Odobel and D. Jacquemin, *J. Phys. Chem. C*, 2012, **116**, 11946–11955.
33 D. Jacquemin, T. Le Bahers, C. Adamo and I. Ciofini, *Phys. Chem. Chem. Phys.*, 2012, **14**, 5383–5388.
34 F. Labat, I. Ciofini and C. Adamo, *J. Mater. Chem.*, 2012, **22**, 12205–12211.
35 G. García, C. Adamo and I. Ciofini, *Phys. Chem. Chem. Phys.*, 2013, **15**, 20210–20219.
36 M. Savarese, P. A. Netti, C. Adamo, N. Rega and I. Ciofini, *J. Phys. Chem. B*, 2013, **117**, 16165–16173.
37 A. D. Becke, *J. Chem. Phys.*, 1993, **98**, 5648.
38 T. Schwabe and S. Grimme, *Phys. Chem. Chem. Phys.*, 2007, **9**, 3397–3406.
39 G. Scalmani, M. J. Frisch, B. Mennucci, J. Tomasi, R. Cammi, and V. Barone, *J. Chem. Phys.*, 2006, **124**, 094107.
40 S. Corni, R. Cammi, B. Mennucci and J. Tomasi, *Phys. Chem. Chem. Phys.*, 2005, **123**, 134512.
41 M. Cossi and V. Barone, *J. Chem. Phys.*, 2001, **115**, 4708.
42 M. Cossi and V. Barone, *J. Chem. Phys.*, 2000, **112**, 2427.
43 Y. Tawada, T. Tsuneda, S. Yanagisawa, T. Yanai and K. Hirao, *J. Chem. Phys.*, 2004, **120**, 8425.
44 T. Yanai, D. P. Tew and N. C. Handy, *Chem. Phys. Lett.*, 2004, **393**, 51.
45 M. J. Frisch, G. W. Trucks, H. B. Schlegel, G. E. Scuseria, M. A. Robb, J. R. Cheeseman, G. Scalmani, V. Barone and et al., *Gaussian 09 Revision A.2*, Gaussian Inc. Wallingford CT 2009.
46 G. Vàmosi, C. Gohlke and R. M. Clegg, *Biophys. J.*, 1996, **71**, 972–994.
47 R. Kubin and A. Fletcher, *J. Lumin.*, 1983, **27**, 455–462.
48 R. Long, N. J. English and O. V. Prezhdo, *J. Am. Chem. Soc.*, 2013, **135**, 18892–18900.
49 R. Improta, *Phys. Chem. Chem. Phys.*, 2008, **10**, 2656–2664.
50 F. Santoro, V. Barone and R. Improta, *J. Am. Chem. Soc.*, 2009, **131**, 15232–15245.